IET Renewable Power Generation

Special Issue on 10th Photovoltaic Science, Application and Technology Conference (PVSAT-10)

IET Journals
The Institution of Engineering and Technology

Optical modelling for concentrating photovoltaic systems: insolation transfer variations with solar source descriptions

ISSN 1752-1416
Received on 4th November 2014
Revised on 23rd January 2015
Accepted on 9th February 2015
doi: 10.1049/iet-rpg.2014.0369
www.ietdl.org

Ian Richard Cole ✉, *Ralph Gottschalg*

Centre for Renewable Energy Systems Technology (CREST), School of Electronic, Electrical and Systems Engineering (SEESE), Loughborough University, Loughborough LE11 3TU, UK
✉ *E-mail: I.R.Cole@lboro.ac.uk*

Abstract: Point source, pillbox and circumsolar ratio-dependent extended light source Sun models are used as solar source inputs into an analytical optical ray trace model for the calculation of plane restricted illumination profiles generated by three example lenses. The example lenses are: a low iron soda-lime glass plano-convex lens, a poly (methyl) methacrylate (PMMA) 3-facet Fresnel lens and a PMMA 20-facet Fresnel lens. Significant differences in illumination profiles are found with solar source description variation. Most notably, it is found that chromatic aberrations and spectrally variant effects specific to the multi-junction solar cell architecture are only identified using the extended light source Sun model. The spectral dependency of material optical properties are analysed in the context of the multi-junction cell architecture by means of spectrally weighted averages corresponding to the active range of the sub-cells.

1 Introduction

Concentrating photovoltaic (CPV) systems typically utilise high-efficiency multi-junction solar cells (MJSCs) for the conversion of solar power to electricity. MJSCs have significantly higher efficiencies than their archetypal counterparts, single-junction solar cells. However, the higher efficiencies of MJSCs are disproportionately reflected in their expense. A major application of MJSCs is found in the space power industry where their expense is of no real concern as their high-power per unit mass ratio takes precedence in design considerations. For the vast majority of terrestrial applications, however, the ratio of primary concern is energy per unit currency. The CPV system offers an economically viable terrestrial application of MJSCs whereby their relative expense is offset by the use of optical concentration systems. This offset by concentration is possible because the multi-junction cell architecture is inherently much more efficient at heat management than the single-junction and thus can withstand much greater light intensities. There are two major elements involved in modelling the behaviour of optical concentration systems, namely: solar source descriptions and concentration components (lenses).

1.1 Solar source descriptions

As witnessed by a static terrestrial observer, the Sun is a bright, hazy circular patch of sky that moves through the visible celestial hemisphere with variations in intensity and colour that are most notable at dawn, midday and dusk. This Sun can be modelled with varying degrees of realism by assertions of approximation. Two extremely common solar source descriptions are the point source and pillbox Sun approximations [1–3]. Less common are extended light source descriptions [4, 5].

1.1.1 Point source Sun: The point source Sun is an approximation to solar irradiation that models the Sun as if all insolation emanates from a single infinitesimally small patch of sky: a point. This is displayed schematically in Fig. 1*a*.

The spatial distribution of insolation is not considered in the point source approximation, hence angular distributions are ignored and the solar beam irradiation is modelled as being emitted from a single point. This point is defined as the location of the solar centre and is often given as an astronomical angle pair, for example, in the form (azimuth, elevation). Spectral distributions can be incorporated into the point source model thus some degree of chromatic aberration analysis can be performed.

The point source Sun is a valid approximation for the analysis of optical systems with very large entry aperture angles, such as flat-plate photovoltaic, for which the entry aperture angle is $\sim\pi^c/2$.

1.1.2 Pillbox Sun: The pillbox Sun is an approximation to solar irradiation that models the Sun as an angular distribution of insolation, with all beam irradiation enveloped by the solar disk. This is displayed schematically in Fig. 1*b*.

The spatial distribution of insolation is then, to some extent, considered in the pillbox approximation. The angular extent of the Sun is typically considered as a radial half-angle of 4.65 mrad, which is the average over the year (see Section 1.1.4, a note on solar angle variations). The distribution of radiation in the pillbox Sun is considered uniform, that is, the radiation intensity at the solar centre is considered equivalent to the radiation intensity at an angular deviation of 4.65 mrad away from the solar centre, beyond which there is zero irradiation. As in the point source Sun, spectral distributions can be incorporated in the model. Some degree of chromatic aberration analysis can be performed. The resultant chromatic aberration analysis will be more accurate in the pillbox approximation than in the point source approximation as a wider angular distribution is considered. Reflection losses from the Fresnel equations and directional changes by refraction will thus be modelled with greater accuracy.

The pillbox Sun may be considered a valid solar model for optical systems in which the entry aperture angles are far greater than that of the Sun.

1.1.3 Extended light source Sun: The extended light source Sun recognises that the distribution of flux intensity within the beam irradiation region is non-uniform. Furthermore, for extended light source Sun models, there is also the recognition that a portion of the beam irradiation lies outside of the solar disk. The portion of beam irradiation external to the solar disk is termed circumsolar radiation. Extended light source solar models are

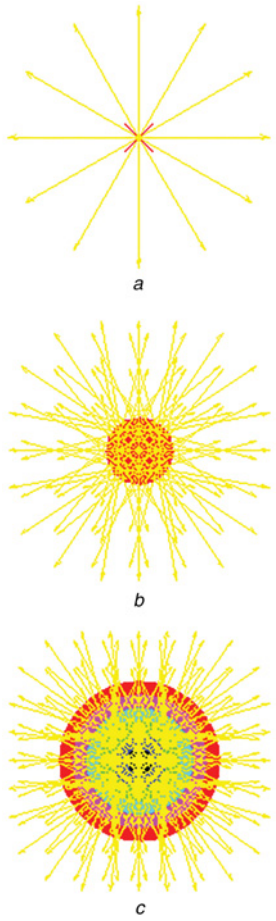

Fig. 1 *Input Suns – solar model schematics*

a Point source Sun
b Pillbox Sun
c Extended light source Sun

typically based on a parameter termed the circumsolar ratio (CSR). The CSR is simply the proportion of beam irradiation contained in the circumsolar region and can be expressed as

$$C = \frac{\int_{\theta_{\text{Sun}}}^{\theta_{\text{Circumsolar}}} \varphi(\theta)\,\mathrm{d}\theta}{\int_{0}^{\theta_{\text{Circumsolar}}} \varphi(\theta)\,\mathrm{d}\theta} \tag{1}$$

where C is the CSR, $\theta_{\text{Circumsolar}}$ is the angular extent of the circumsolar region, θ_{Sun} is the angular extent of the solar disc, φ is the solar flux intensity and θ is the angular deviation from the solar centre.

An example extended light source Sun model using CSR as the primary input parameter is the Buie *et al.* model [4], which is based on observations of the Lawrence Berkley Laboratory (LBL) [6]. The extended light source Sun model is shown schematically in Fig. 1*c*.

The spectral content of the central solar and circumsolar regions are significantly different. These spectra can be modelled independently using, for example, Simple Model of the Atmospheric Radiative Transfer of Sunshine [7]. Spatially dependent spectral inclusion is thus possible using an extended light source Sun model. The spectral effects of CSR variation are significant, as shown in Fig. 2.

The average photon energy (APE) is a useful metric for the consideration of spectral variation, although it does somewhat simplify the mechanisms behind the average shift.

There are many CPV systems with input aperture half angles in the sub-degree range. For these systems, extended light source Sun models are necessary for the accurate prediction of system

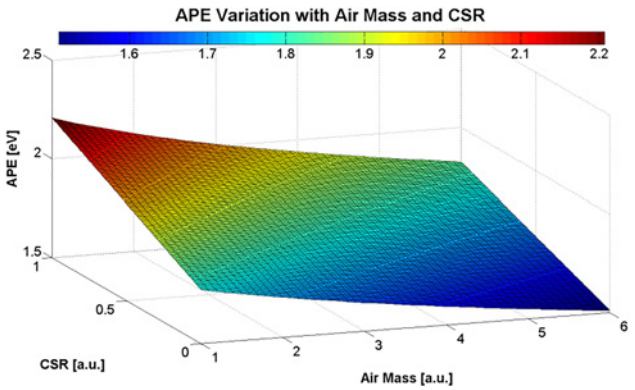

Fig. 2 *APE variation with air mass and CSR*

performance as the use of point source and pillbox Sun models results in overestimations of system performance [8, 9].

1.1.4 Note on solar angle variations: The angular extent of the solar disk varies with distance from the Sun according to

$$\delta = \tan^{-1}\left(\frac{d}{2D}\right) \tag{2}$$

where δ is the apparent angular solar radius, d is the diameter of the Sun and D is the Sun–Earth distance.

Owing to the elliptical orbit of the Earth, the Sun–Earth distance varies by 3% over the year. Accordingly, from (2), the apparent angular solar radius varies from aphelion to perihelion between 4.584 and 4.742 mrad. The angular solar radius is often quoted as 4.65 mrad [10, 11]. This is the angular radius at a Sun–Earth distance of 1 astronomical unit (au), which is the yearly average. Good arguments exist for the inclusion of such variations in extended light source modelling [5], namely, that calculated CSR changes with defined central solar boundaries.

1.2 Concentrating lenses

The two major lenses used in CPV systems are the Fresnel lens and the plano-convex lens. The Fresnel lens is used as the primary concentration device and the plano-convex lens as a secondary concentrator. Secondary concentrators are used in CPV to reduce the effects of lateral deviations in the focal point because of errors in solar tracking.

1.2.1 Plano-convex lens: Arguably, the archetypal lens is the plano-convex lens. The standard plano-convex lens is essentially a spherical cap with a cylindrical back section. Using these geometric sections, the description of a plano-convex lens can be reduced to three parameters, as shown in Fig. 3*a*. The three parameter description of the plano-convex lens is useful when modelling it as a three-dimensional (3D) object positioned relative to other objects in 3D space.

Like all lenses, the plano-convex lens suffers aberrations both spherical and chromatic. The spherical aberrations of an example plano-convex lens are shown in a 2D ray trace diagram in Fig. 4*a*.

Fig. 4*a* shows light rays from infinity traced through a plano-convex lens. The black lines represent rays inside the lens and the red lines represent rays that have left the lens. The lens parameters used in this example are: $(R, C, D) = (20, 17.3, 17.3)$. The rays that enter the lens near its centre focus further from the lens back than the rays entering the lens near its edge. The chromatic aberration effect is similar, with the higher wavelength light focusing further from the lens back than the lower wavelength light. This results from the spectral dependency of the refractive index.

A typical material choice for the plano-convex secondary lens is low iron soda-lime glass. The optical properties of low iron soda-lime glass are given in Section 2.1.

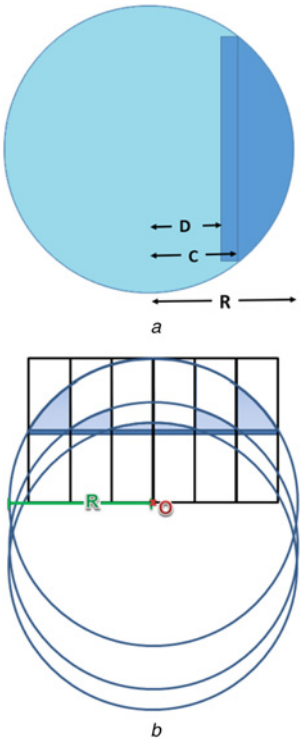

Fig. 3 *Plano-convex and Fresnel design bases – geometric principles*

a Plano-convex shell
b Fresnel shell

As well as being the choice secondary concentration device for some CPV systems, the plano-convex lens is sometimes used as an approximate model for more geometrically complex primary concentration lenses, although it is rarely practically used as such.

1.2.2 Fresnel lens: The Fresnel lens is the most prolific primary optical concentration device in high concentration photovoltaic (HCPV) systems today. An ideal Fresnel lens is considered herein. Structurally, the ideal Fresnel lens can be considered as a material reduction of a plano-convex lens comprising concentric circular facets with surfaces parallel to the plano-convex lens front, as shown in Fig. 3*b*. Given the plano-convex design base, the ideal Fresnel lens can be described with four parameters – the three parameters of the plano-convex description and the number of facets, n. This proves a useful description in 3D modelling.

Like all lenses, the Fresnel lens suffers aberrations both spherical and chromatic. The spherical aberrations of an example Fresnel lens are shown in a 2D ray trace diagram in Fig. 4*b*.

Fig. 4*b* shows light rays from infinity traced through a 3-facet Fresnel lens. The black lines represent rays inside the lens and the red lines represent rays that have left the lens. The lens parameters used in this example are: $(R, C, D, n) = (20, 17.3, 17.3, 3)$.

The Fresnel lens behaves similarly to the plano-convex for incident paraxial light with the added practical benefits of a reduction in mass and an increase in power transmission because of reduced material traversal path lengths. An optical dissimilarity is the image distortion resulting from the Fresnel facet arrangement. This is an ambiguous issue in CPV and more generally in standard optical modelling whereby a degree of 'haze' is introduced to the image to account for the facet distortions.

A typical material choice for the Fresnel primary lens is poly (methyl) methacrylate (PMMA). The optical properties of PMMA are given in Section 2.2. A common alternative material choice for the Fresnel lens is silicone on glass. Silicone material properties are not discussed herein, although the spectrally banded material parameter descriptions presented in Section 2 can be applied to any given material.

1.3 CPV modelling

Given that the validity of approximated solar source descriptions is called into question when modelling optical systems with small entry apertures, CPV, particularly HCPV – where input aperture half angles are often in the sub-degree range, system modelling requires the use of extended light source Sun descriptions in order to accurately identify the MJSC illumination profiles.

This paper offers a ray trace investigation and analysis of three example lenses using three different solar source descriptions. The investigation herein is spectrally banded and weighted according to

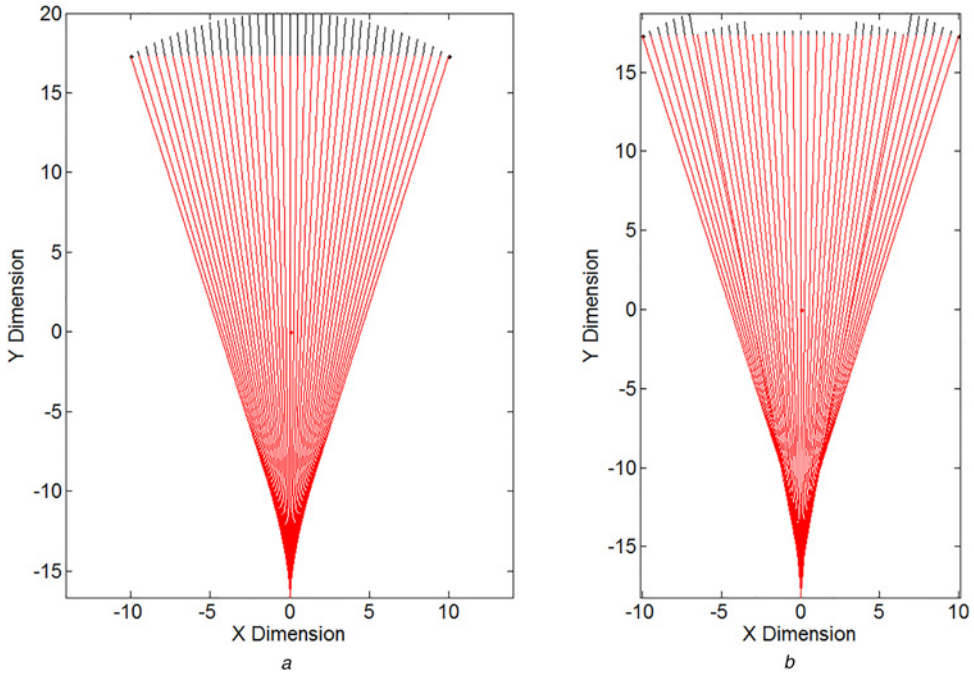

Fig. 4 *2D Point source ray trace diagrams, for example, plano-convex and Fresnel lenses*

a Plano-convex 2D ray trace
b Fresnel 2D ray trace

IET Renew. Power Gener., 2015, Vol. 9, Iss. 5, pp. 412–419

a typical multi-junction cell architecture. That is, an approximation to the active sub-cell ranges [11] of 280–680, 680–880 and 880–1880 nm. This allows for an investigation of chromatic aberrations in the specific context CPV.

2 Material properties

The primary material properties of concern when considering lens-based optical systems are the absorption coefficient and the refractive index.

The absorption coefficient is directly related to intensity reduction by material traversal according to the Beer–Lambert law

$$T = \frac{I}{I_0} = \mathrm{e}^{-\alpha l} \tag{3}$$

where T denotes transmissivity; I and I_0 denote the intensity of transmitted and incident light, respectively; αdenotes the absorption coefficient; and l denotes the material traversal path length.

The refractive index is directly related to reflection losses by the Fresnel (4)–(6) and directional change by Snell's law (7)

$$R = \frac{R_s + R_\mathrm{p}}{2} \tag{4}$$

where R denotes the reflection coefficient, R_s denotes the reflectance for light polarised perpendicular to the material interface normal and R_p denotes the reflectance for light polarised parallel to the material interface normal

$$R_s = \left(\frac{n_1 \cos \theta_\mathrm{i} - n_2 \cos \theta_\mathrm{t}}{n_1 \cos \theta_\mathrm{i} + n_2 \cos \theta_\mathrm{t}}\right)^2 \tag{5}$$

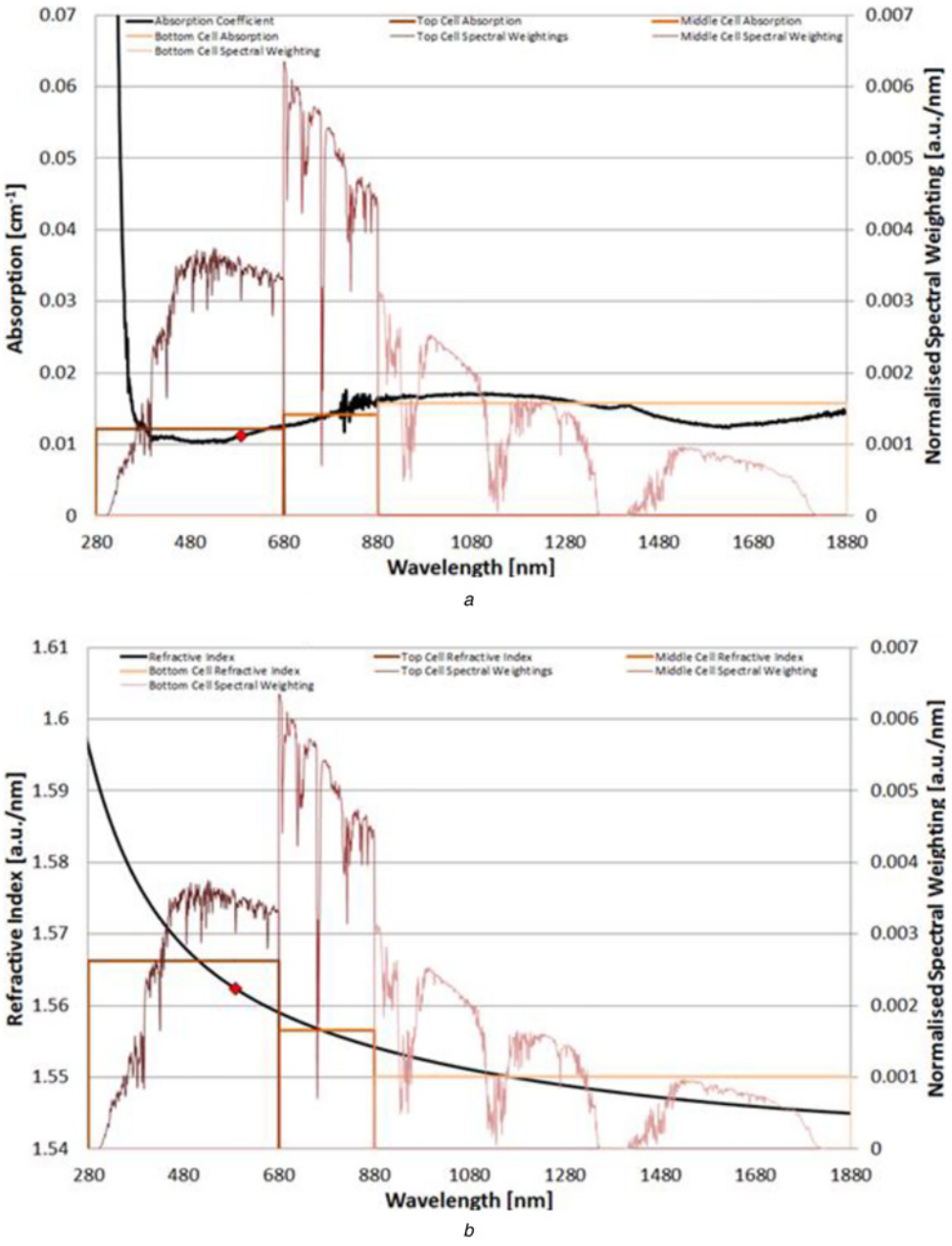

Fig. 5 *Low iron soda-lime glass material properties*

a Absorption coefficient
b Refractive index

$$R_p = \left(\frac{n_1 \cos \theta_t - n_2 \cos \theta_i}{n_1 \cos \theta_t + n_2 \cos \theta_i} \right)^2 \quad (6)$$

$$n_1 \sin \theta_i = n_2 \sin \theta_t \quad (7)$$

where n_1 denotes the refractive index of the primary material, n_2 denotes the refractive index of the secondary material, θ_i denotes the incident angle to the material interface normal and θ_t denotes the transmission angle to the material interface normal.

Two materials are here considered. The typical materials of plano-convex and Fresnel lenses are low iron soda-lime glass and PMMA, respectively. The material absorption and refraction data presented herein is as measured at Loughborough University by spectrophotometry and ellipsometry, respectively. The noise in the absorption curve at about 800 nm is because of a change of sensor in the spectrophotometer. All material properties are shown with spectrally weighted averages relating to the AM1.5D solar spectrum, for illustration.

2.1 Low iron soda-lime glass

Low iron soda-lime glass is the glass choice of preference in many optical applications because of its reduced tinting and increased transmission properties. The absorption coefficient and refractive index of low iron soda-lime glass are shown in Fig. 5. Nominal values at 589 nm are highlighted for reference.

Low iron soda-lime glass has a particularly low absorption coefficient, especially from 350 nm onwards where it is also notably flat. The refractive index follows the standard form of material refractive indices – higher at low wavelengths, flattening to lower at high wavelengths.

2.2 PMMA

PMMA is the predominant material of Fresnel lenses for CPV. The material is preferable because of its low weight. The absorption

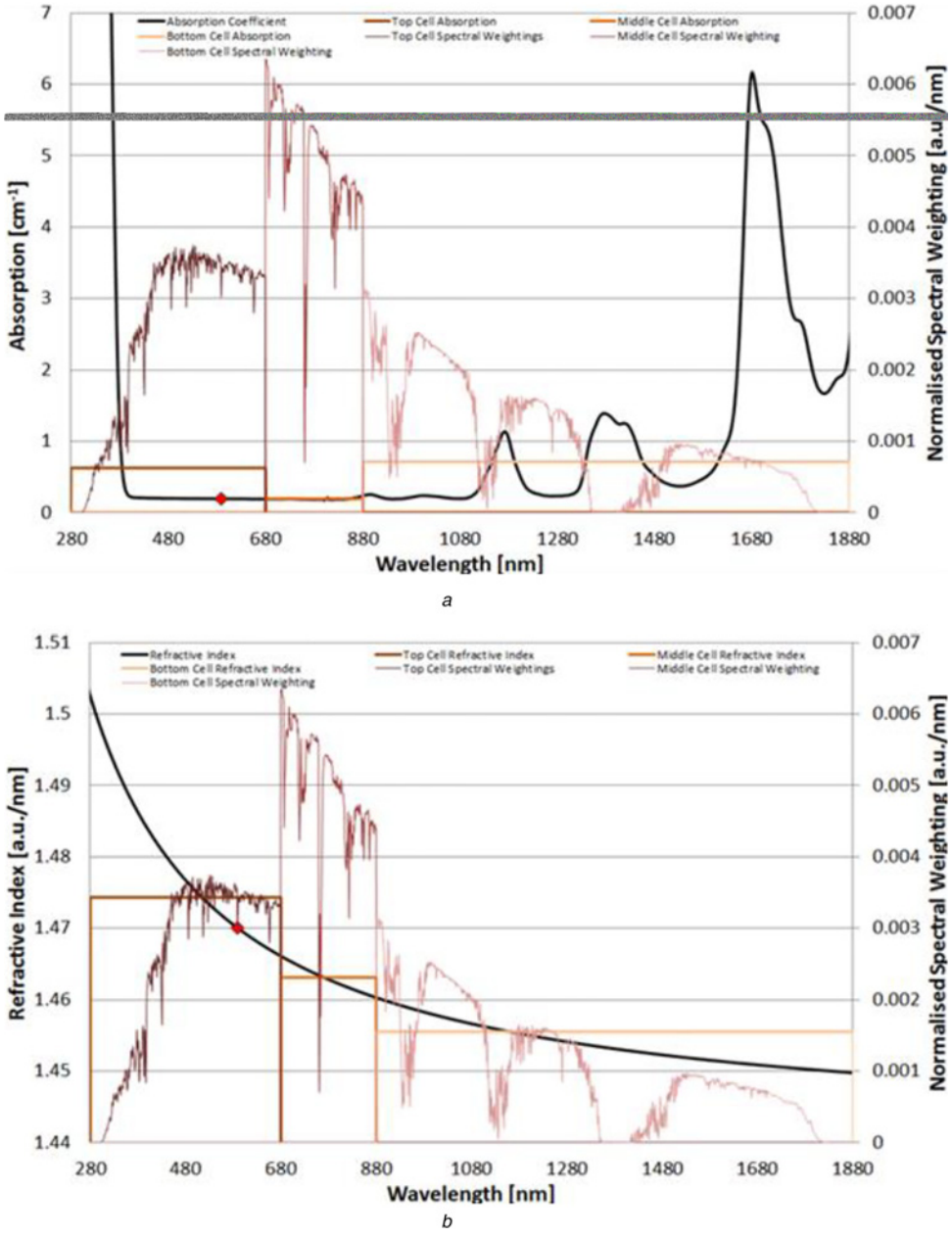

Fig. 6 *PMMA material properties*

a Absorption coefficient
b Refractive index

IET Renew. Power Gener., 2015, Vol. 9, Iss. 5, pp. 412–419

Table 1 Nominal and banded average material optical properties of low iron soda-lime glass and PMMA

Reference	Low iron soda-lime glass		PMMA	
	Absorption, cm^{-1}	Reference index, au	Absorption, cm^{-1}	Reference index, au
nominal 589 nm	0.011	1.562	0.195	1.47
whole cell	0.014	1.56	0.516	1.467
top cell band	0.012	1.566	0.624	1.474
middle cell band	0.014	1.557	0.192	1.463
bottom cell band	0.0156	1.55	0.714	1.456

coefficient and refractive index of PMMA are shown in Fig. 6. Nominal values at 589 nm are highlighted for reference.

The absorption coefficient of PMMA shows that the material is practically opaque until 400 nm. From thereon the absorption coefficient is flat until the bottom band region where it peaks and troughs, raising the average value dramatically. The refractive index follows the standard form of material refractive indices – higher at low wavelengths, flattening to lower at high wavelengths.

The sub-cell banded, whole cell banded and 589 nm nominal material properties are listed in Table 1.

It can be seen from Table 1 that the spectral variations in absorption coefficient for PMMA result in significantly different weighted averages for the banded spectral analysis. Spectrally dependent phenomena such as this can play significant roles in CPV system performance because of the spectral sensitivity of MJSCs.

3 Illumination profiles

Three example lenses have been simulated in this investigation, namely: a low iron soda-lime glass plano-convex lens, a 3-facet PMMA Fresnel lens and a 20-facet PMMA Fresnel lens. These example lenses prove adequate for demonstrating model limitations and profile variations, although it should be noted that CPV systems tend to use primary Fresnel lenses with 100 or more facets. The illumination profile is calculated at the focal length as calculated by the plano-convex reduced form of the lens maker's equation

$$F = \frac{R}{(n-1)} \tag{8}$$

where F is the focal length of the lens, R is the radius of the convex lens front and n is the nominal refractive index of the material as quoted at 589 nm.

One of the main drivers for the use of the Fresnel lens in CPV optical systems is its reduced volume and thus material mass and cost. The volume of a Fresnel lens is inversely exponentially correlated to the number of facets. The relative volumes of a plano-convex, 3-facet Fresnel and 20-facet Fresnel lens are ~1, 0.5 and 0.1, respectively.

For reference, the three example lenses simulated here use the same plano-convex shell. That is the shell as described in Section 1.2: $(R, C, D) = (20, 17.3, 17.3$ cm).

The three example lenses are simulated here in ideal optical alignment conditions, such that the lens front is normal to the Sun, commonly referred to as ideal solar tracking. As such, the resultant illumination profiles are radially symmetrical about a central point, thus a 2D cross-section offers a sufficient description for their presentation. The term 'deviation from centre' on the x-axis of Figs. 7–12 thus refers to the distance from the central point of the profile. Illumination profiles are given here in both absolute and normalised forms. The absolute forms show the average irradiance in watt per square metre of a given annulus for each spectral band of the radially symmetrical profile. The normalised forms present the irradiance profiles of each spectral band relative to their maximum intensity. The normalised forms are particularly useful for chromatic aberration analysis as spectrally specific illumination variations are easily identified. In all cases, the AM1.5D spectrum was used for illustration and consistency with the data presented herein. The extended light source profile uses a CSR of 0.27. All results presented here are as simulated by ray-tracing using a bespoke, in-house, simulation tool developed at Centre for Renewable Energy Systems Technology.

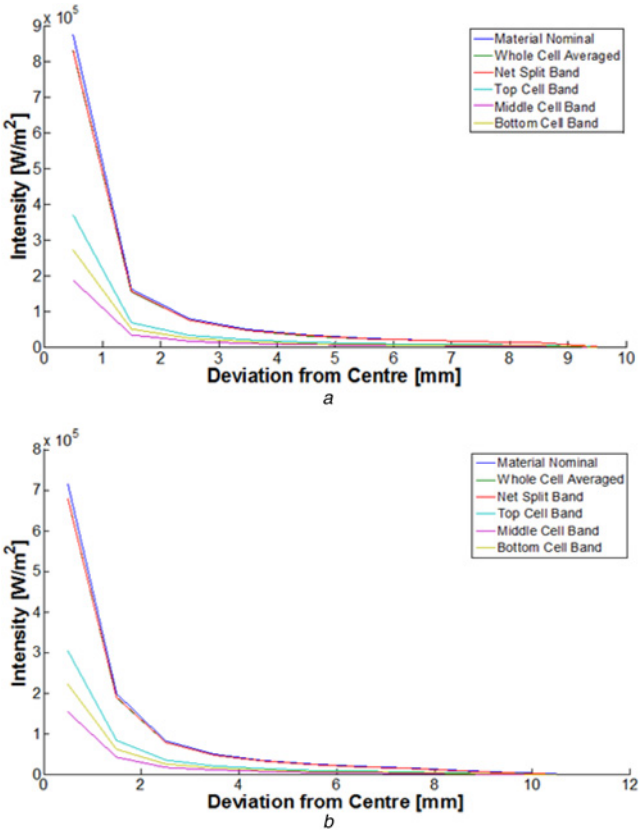

Fig. 7 *Plano-convex banded point source and pillbox traces*

a Point source
b Pillbox

3.1 Plano convex trace

The ray trace illumination profile results for the low iron soda-lime plano-convex lens are presented here using each of the three solar source descriptions: the point source Sun, the pillbox Sun and the extended light source Sun.

The absolute banded point source (Section 1.1.1) and pillbox (Section 1.1.2) Sun traces are presented in Fig. 7. The absolute and normalised banded extended light source (Section 1.2.3) trace is shown in Fig. 8.

The plano-convex lens was traced here using three different solar source descriptions. The illumination profiles for the point source, pillbox and extended light source Sun models show significant differences. The point source Sun trace overestimates maximum intensity and underestimates spread. The pillbox source underestimates both maximum intensity and spread. Spectrally banded differences in intensity profiles are mostly ignored in both the point source and pillbox Sun traces.

3.2 3-Facet Fresnel traces

The ray trace illumination profile results for the PMMA 3-facet Fresnel lens are presented here using each of the three solar source descriptions: the point source Sun, the pillbox Sun and the extended light source Sun.

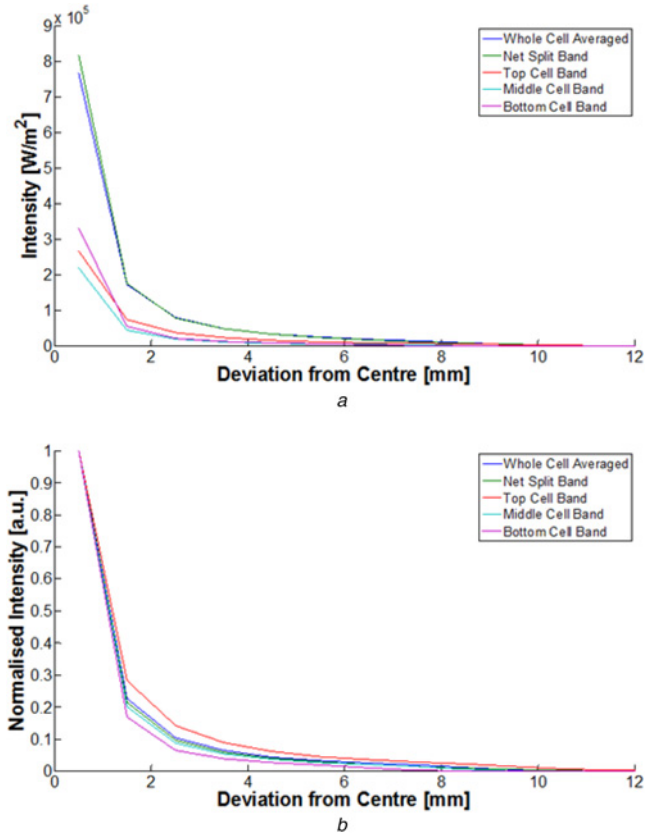

Fig. 8 *Plano-convex extended light source trace*

a Absolute
b Normalised

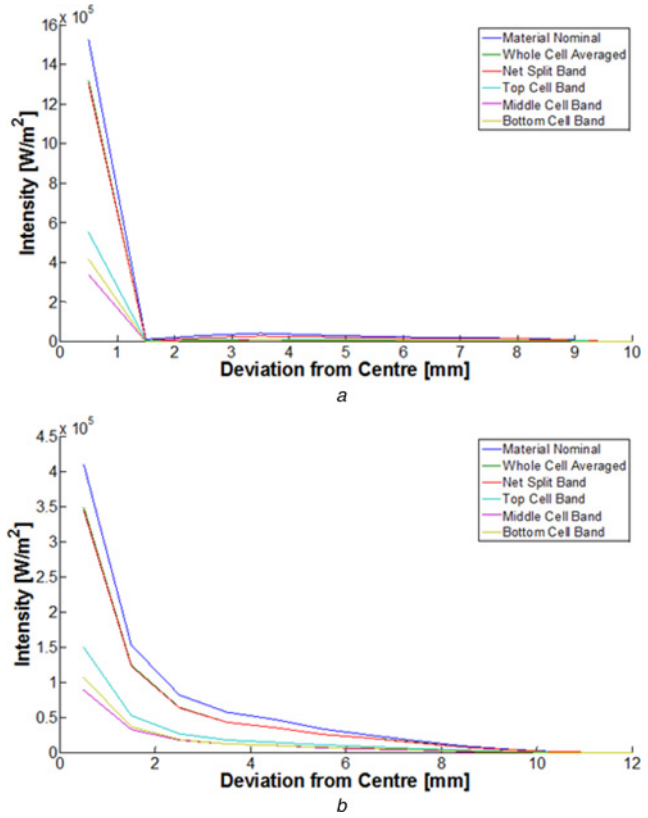

Fig. 9 *3-Facet Fresnel banded point source and pillbox traces*

a Point source
b Pillbox

The absolute banded point source (Section 1.1.1) and pillbox (Section 1.1.2) Sun traces are presented in Fig. 9. The absolute and normalised banded extended light source (Section 1.2.3) trace is shown in Fig. 10.

The 3-facet Fresnel lens was traced here using three different solar source descriptions. The illumination profiles for the point source, pillbox and extended light source Sun models show significant differences. The point source Sun trace dramatically overestimates (~3x) maximum intensity and underestimates spread. The pillbox source underestimates both maximum intensity and spread. Spectrally banded differences in intensity profiles are found in both the point source and pillbox Sun traces yet they are very small when compared with the differences found in the extended light source Sun trace.

3.3 20-Facet Fresnel traces

The ray trace illumination profile results for the PMMA 20-facet Fresnel lens are presented here using each of the three solar source descriptions: the point source Sun, the pillbox Sun and the extended light source Sun.

The absolute banded point source (Section 1.1.1) and pillbox (Section 1.1.2) Sun traces are presented in Fig. 11. The absolute and normalised banded extended light source (Section 1.2.3) trace is shown in Fig. 12.

The 20-facet Fresnel lens was traced here using three different solar source descriptions. The illumination profiles for the point source, pillbox and extended light source Sun models show significant differences. The point source Sun trace dramatically overestimates (~3×) maximum intensity and underestimates spread. The pillbox source underestimates both maximum intensity and spread. Spectrally banded differences in intensity profiles are found in both the point source and pillbox Sun traces yet they are very small when compared with the differences found in the extended light source Sun trace.

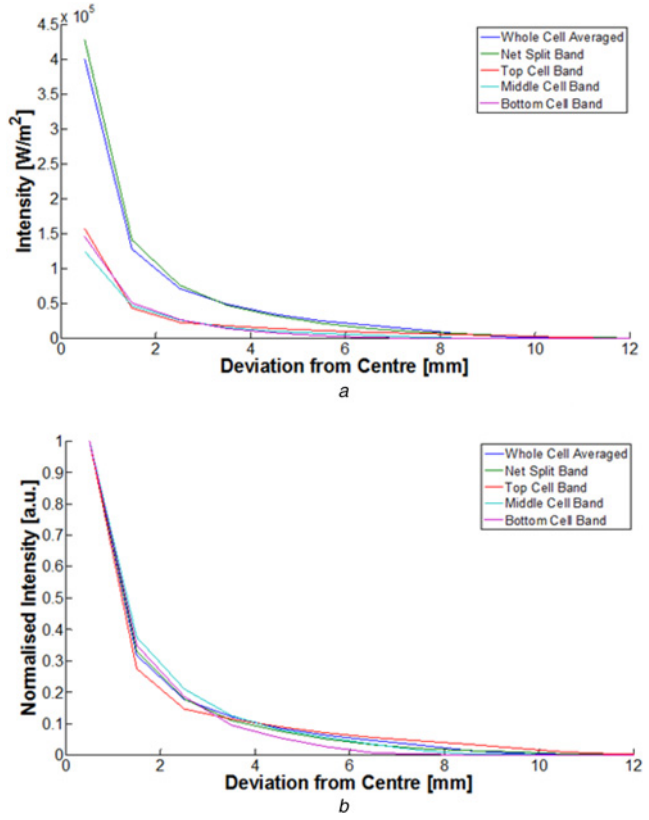

Fig. 10 *3-Facet Fresnel extended light source trace*

a Absolute
b Normalised

IET Renew. Power Gener., 2015, Vol. 9, Iss. 5, pp. 412–419

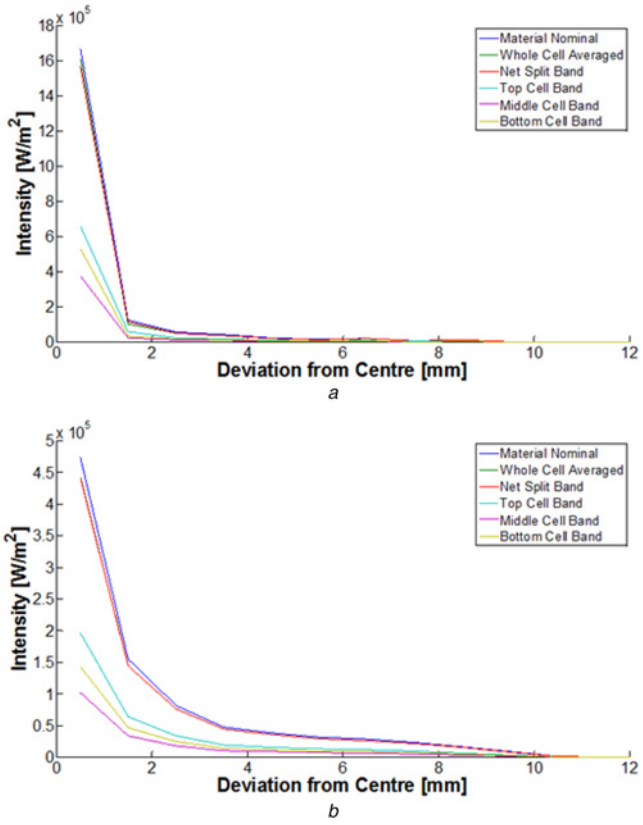

Fig. 11 *20-facet Fresnel banded point source and pillbox traces*

a Point source
b Pillbox

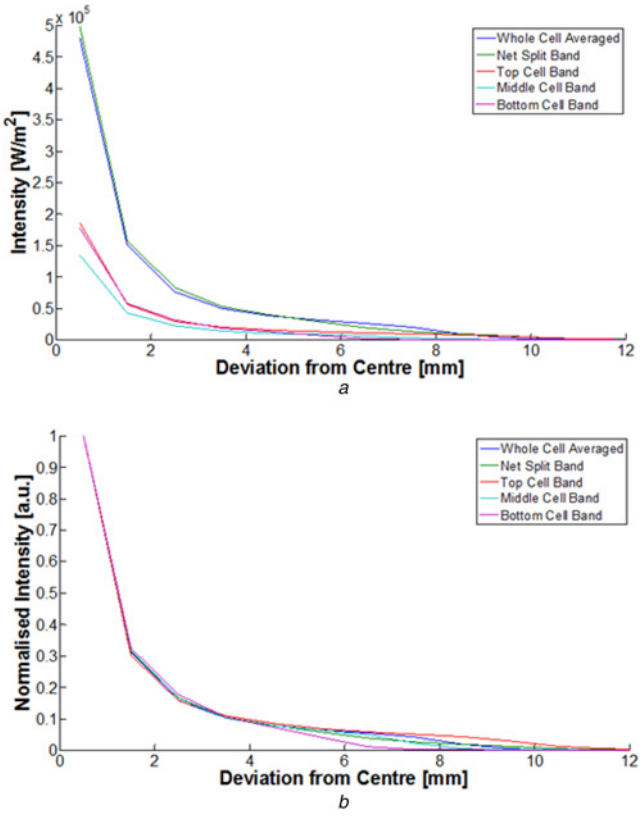

Fig. 12 *20-facet Fresnel extended light source trace*

a Absolute
b Normalised

4 Summary

The importance of using realistic solar source descriptions in CPV optical system simulations has been highlighted. Three different source descriptions show notable differences when used as illumination sources for different lenses.

Owing to the spatially distributed bi-regional nature of the solar beam spectrum, spectrally resolved optical phenomena such as chromatic aberration is not thoroughly investigated unless an extended light source Sun model is used. The spectra in these models can be separated according to the CSR. The importance of modelling the spectral distribution of incident irradiation is elevated when considering the current limiting effects of MJSCs.

In the soda-lime glass plano-convex lens, the point source and pillbox traces show next to no chromatic aberration effects because of near constant nature of the material absorption coefficient. The extended light source Sun trace, however, shows notable banded intensity variations resulting from the large differences in circumsolar contributions over the sub-cell band ranges.

In the PMMA Fresnel lenses, the point source traces show varied small spectral deviations for the 3-facet lens and slightly larger spectral deviations in the 20-facet lens. This difference can be attributed to an increase in reflections off inner facet Fresnel walls which are more obvious in point source traces as the beam spread is much less. The pillbox traces show small spectral deviations in the 3-facet lens and near to no spectral variations in the 20-facet lens. This can be attributed to reduction in variation by absorption with the increase in number of facets. Finally, the extended light source traces show large near centre spectral variations and large near edge variations spectral variations for the 3-facet lens, whereas for the 20-facet lens the near central variations are smaller and the near edge variations are larger. This can be attributed to the reduction in variation by absorption and the increase in spread by reflection with the increase in number of facets.

Generally speaking, a Fresnel lens with a low number of facets show significant normalised intensity variations over the full spread of the image. As the number of facets in the Fresnel lens is increased, the near centre variations reduce because of the reduction in lens thickness, whereas the variations further from the centre increase because of an increase in facet wall reflections. These phenomena are only notable when considering the Sun as an extended light source. Extended light source Sun models are thus crucial to the optimisation of HCPV system optics.

It is also shown here that, despite being derived from its base form, the Fresnel lens is not well approximated in optical simulation by the plano-convex equivalent.

5 References

1 Roccia, J., Piaud, B., Coustet, C., *et al.*: 'SOLFAST, a ray-tracing Monte-Carlo software for solar concentrating facilities'. Journal of Physics Conf. Series, 2012
2 Shea, S.: 'Evaluation of glare potential for photovoltaic installations' (Suniva, Inc., Norcross, USA, 2012)
3 Lovegrove, K., Pye, J.: 'Fundamental principles of concentrating solar power systems', in Lovegrove, K., Stein, W. (Eds.): 'Concentrating solar power technology' (Woodhead Publishing Limited, Philadelphia, USA, 2012), pp. 16–67
4 Buie, D., Monger, A., Dey, C.: 'Sunshape distributions for terrestrial solar simulations', *Sol. Energy*, 2003, **74**, pp. 113–122
5 Neumann, A., Witzke, A., Jones, S., Schmitt, G.: 'Representative terrestrial solar brightness profiles', *Sol. Energy*, 2002, **124**, (2), pp. 325–333
6 McMahon, W., Kurtz, S., Emery, K., Young, M.: 'Criteria for the design of GaInP/GaAs/Ge triple-junction cells to optimize their performance outdoors'. NREL/CP-520-33554, NREL, CO, USA, 2003
7 Gueymard, C.: 'SMARTS, a simple model of the atmospheric radiative transfer of sunshine: algorithms and performance assessment'. FSEC-PF-270-95, Florida Solar Energy Center, Cocoa, FL, USA, 1995
8 Schubnell, M.: 'Sunshape and its influence on the flux distribution in imaging solar concentrators', *ASME J. Solar Energy Eng.*, 1992, **114**, (4), pp. 260–266
9 Cole, I., Betts, T., Gottschalg, R.: 'Solar profiles and spectral modelling for CPV simulations', *IEEE J. Photovolt.*, 2012, **2**, (1), pp. 62–67
10 Puliaev, S., Penna, J.L., Jilinski, E.G., Andrei, A.H.: 'Solar diameter observations at Observatório Nacional in 1998-1999', *Astron. Astrophys. Suppl.*, 2000, **143**, (2), pp. 265–267
11 Thuillier, G., Sofia, S., Haberreiter, M.: 'Past, present and future measurements of the solar diameter', *Adv. Space Res.*, 2005, **35**, pp. 329–340